OPTIMIZATION OF PATCH SHAPE FOR FGM PLATES USING THE NSGA-II ALGORITHM

Soufiane ABBAS[*/], Mohamed Ikhlef CHAOUCH[*], Hinde LAGHFIRI[***], Mohamed BENGUEDIAB[**]**

[*]Center of Research in Mechanics, University of Constantine 1, Crm, Po Box 73 B, 25000, Constantine, Algeria
[**]Laboratory of Materials and Reactive Systems, University Djillali Liabes of Sidi Bel Abbes, Bp 89, Lmsr, 22000, Sidi Bel Abbes, Algeria
[***]GC Laboratory, Mohammadia School of Engineering, Mohammed University in Rabat, Ibn Sina, Rabat, 10080, Rabat, Morocco

abbas.s@crm-constantine.dz, ikhlefchaouch.m@crm-constantine.dz, hindelaghfiri2014@gmail.com, benguediabm@gmail.com

received 28 January 2025, revised 09 October 2025, accepted 19 October 2025

Abstract: In advanced composite structures, optimizing patch shapes is an important step towards improving the mechanical performance of Functionally Graded Materials (FGMs). The optimization of patch shapes was presented in this research for FGM plates using an evoltionary algorithm method specifically the Non-dominated Sorting Genetic Algorithm II (NSGA-II) with a Pareto front. The purpose of the optimization was to minimize the mode I stress intensity factor (K1), an important contributor to crack growth and the overall integrity of structure. A multi-objective optimization was conducted with multiple patch designs. K1 was reduced between 0.95% to 70% while maintaining the toughness of the plate some cases and varying the load condition on others. This suggests that the optimized patch shapes are capable of minimizing stress concentration and increasing the durability of FGM plates. This study has established a strong foundation for future research to be conducted on optimized patch shapes for FGMs.

Key words: FGM, Evolutionary algorithm, NSGA-II, Pareto Front Analysis, Crack Propagation

1. INTRODUCTION

Functionally Graded Materials (FGMs) are an increasing component of the aerospace industry applying for design and structural support in contemporary aircraft and spacecraft owing to their capabilities of handling extreme thermal and mechanical stresses [1,2]. FGMs can be applied as a material property can gradually change over a small distance, unlike aluminum, a traditional homogenous material that has been used as a structural material in aircraft since the usage of aluminum became commonplace in the industry [3]. FGMs can meet the demands of use as materials are better suited to bridge extreme temperature gradients and implications from localized mechanical loads. These applications include thermal coatings for jet engines turbine or combustion chambers (for example) leading edges of the wing of the aircraft (for example), critical fuselage structures in military aircraft. In these applications, FGMs work to diffuse stresses and resist delamination and thermal degradation thus contributing to durability and safety and weight reduction with the structures. Compared to aluminum, which is another traditional material, FGMs offer a range of transformative benefits [4].

These FGMs exhibit a gradual change in composition that leads to gradual variations in their mechanical, thermal, and chemical properties. This design is directed toward reducing thermal stresses and mechanical mismatches, which makes FGMs well suited for applications requiring premier performance in harsh environments [5,6]. Research has studied coupling Aluminum (Al) and Zirconium (Zr). Aluminum offered solid strength and flexibility while zirconium provided heat resistance and toughness. They can be applied in aerospace, automotive manufacturing, and medical engineering. For example, Al/Zr FGMs functioning as heat shield coatings in jet engines and gas turbines, brake discs in car systems, and body-friendly materials for dental implants and joint replacements [7–10]. But still, implantation of FGMs shows damage when under stresses repeated or high temperature, making their structure weak [11,12]. To solve the issue, engineers come up with composite patches of CFRP. Studies show that these patches can recover strength and prolong the life of a cracked part [13–15]. According to Karuppannan et al. (2013), CFRP patches are effective for the repair of aircraft wings, whereas Brandtner-Hafner (2024) has utilized these patches to strengthen bridges, Reis et al. (2022) having applied them to reinforce pipes [16–18]. Carbon-fiber patches do not only act as an overlay; they also ensure distributed stress thereby arresting crack propagation. But it is still difficult to form these patches into suitable profiles and place the material in right locations; this also affects their performance [15,19,20].

The finite element method (FEM) is vital for the modelling of cracked functionally graded materials (FGMs). It explores the different states of stresses, quality of crack paths, and the evaluation of stress intensity factors (K1) among other variables. Being the early stage in indicating the severity of a crack, the effort to reduce the value of K1 is very important in enhancing patch design. To a large extent, there exists an innate challenge regarding the choice of the patch shape. However, a balance has to be struck between the stress-reduced patch and material saving [21]. Classical FEM investigations have considerably cast light upon how patches perform, yet they provide relatively little insight on the best choices.

In their bid to overcome the challenges, researchers are increasingly coupling FEM with optimization techniques grounded in evolutionary algorithm. The Non-dominated Sorting Genetic Algorithm II (NSGA−II) is particularly recommended for a multi- objective optimization problem. NSGA−II works miracles in resolving a trade-off among conflicting objectives-using the exciting tricks of the

DOI 10.2478/ama-2025-0087

Pareto front. They are using Yang and their team in 2024. They took NSGA−II and basically optimized the geometrical patch shape for repair direction it extended the lifetimes of structures until they finally became fatigued. Then they did something interesting. The NSGA−II and Finite Element Method (FEM) were used in combination to model the fiber orientations inside a composite to lower K1 and increase workability [22,23].

In this study, we combine FEM simulations with NSGA−II optimization to identify the best shapes for carbon fibre patches on cracked Al/ZrO2 FGMs. To this end, the aim is to lessen K1 through Pareto front optimization. This good method gives a strong basis on which to relate mechanical performance to material application, thereby improving the reliability of repairs applied to FGMs. Research results will provide an orderly improvement for this crack repair method applied to FGMs in many areas, giving useful ideas for the design and tweaking of high-quality patch solutions.

Recently, the Non-dominated Sorting Genetic Algorithm II (NSGA-II) has become a widely used multi-objective optimization tool due to its ability to generate a set of optimal trade-off solutions to solve complex and often conflicting objectives. Numerous industrial studies have demonstrated the reliability and capability of the algorithm to solve optimization problems in hope of satisfying multiple criteria for performance. For example, Zhang et al. [24]. presented a study combining numerical simulation, response surface methodology (RSM), and NSGA-II to optimize low-pressure casting parameters for large aluminum alloy wheels. A key finding was the significant improvement in cast quality, which was consistently reported from simulations and confirmed from experiments. Likewise, Wang et al. [25], showed how NSGA-II could be applied to optimize laser cleaning parameters for Q390 steel and achieve efficient rust removal with a clean surface for pre-welding. In another case, Montgomery et al. [26] provide a case study reporting NSGA-II was better than traditional methods to develop robust experimental designs for mixture experiments under manufacturing tolerances, demonstrating greater statistical stability and process reliability. Additionally, Sharma et al. [27] assessed the sensitivity of NSGA-II to its internal parameters during the optimal design phase of water distribution systems to characterize the effect of the population size and subsequently established guidelines for practitioners to increase the efficiency of the algorithm. Likewise, Li et al. [28] coupled a backpropagation (BP) neural network with NSGA-II to allow the structure of a Giant Magnetostrictive Actuator (GMA) to be optimized with respect to intensity, uniformity, and coil losses verified through prototype data. Collectively, these investigations reinforce the versatility and adaptability of NSGA-II, in particular as a hybridization of modeling, artificial intelligence, and simulation methods to solve multi-objective optimization problems across a wide range of engineering scenarios.

In this study, finite element method (FEM) simulations are integrated with the Non-dominated Sorting Genetic Algorithm II (NSGA-II) to determine the optimal geometrical shapes of carbon fiber composite patches for repairing cracked Al/ZrO_2 functionally graded material (FGM) plates. The primary objective is to minimize the stress intensity factor (K_1) through Pareto front optimization, thereby establishing a strong correlation between mechanical performance and material application. This integrated approach enhances the reliability of FGM repair strategies and provides valuable insights for the design and optimization of high-performance composite patch solutions. The novelty of this work lies in the application of NSGA-II for the automatic exploration of a wide range of potential patch geometries and the identification of the optimal configuration within a reduced computational time. Unlike traditional methods that depend on predefined geometries such as rectangular, diamond, or elliptical shapes, the proposed methodology offers superior flexibility, efficiency, and precision in optimizing composite patch designs for functionally graded materials.

2. ANALYTICAL PACKGROUND

The variation of material properties across the thickness is determined using two homogenization methods: a power-law model and an exponential model. The power-law model expresses the effective properties of FGM plates based on the framework outlined [29,30] (Fig. 1).

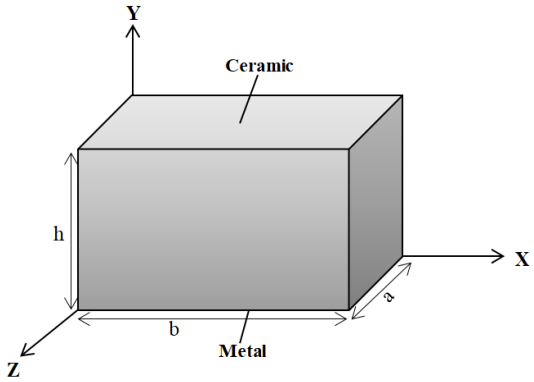

Fig. 1. Geometry of a functionally graded material plate

$$P(z) = (P_c - P_m)V_c + P_m \tag{1}$$

P_c and P_m represent the Young's modulus (E), Poisson's ratio (ν), and mass density (ρ) of the ceramic and metal materials, located at the top and bottom surfaces of the plate, respectively. The volume fraction of the ceramic material, V_c is expressed as:

$$V_c = (\frac{Z}{h})^p \tag{2}$$

where (p) is the power-law index, a positive parameter that controls the material distribution across the thickness $Z \in [0, h]$.

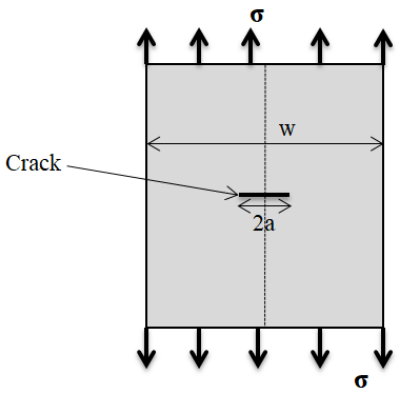

Fig. 2. Illustration of a cracked plate with width w and crack length 2a

The theory of elasticity for isotropic materials forms the foundation of fracture mechanics, with a primary focus on stress concentration at the crack tip. As the radial distance (r) from the crack tip approaches zero, the stress theoretically tends toward infinity,

rendering conventional stress calculations impractical.

$$\sigma_{XX} = \frac{K_1}{\sqrt{2\pi r}}\cos\frac{\theta}{2}\left[1 - \sin\frac{\theta}{2}\sin\frac{3\theta}{2}\right] \quad (3)$$

$$\sigma_{YY} = \frac{K_1}{\sqrt{2\pi r}}\cos\frac{\theta}{2}\left[1 + \sin\frac{\theta}{2}\sin\frac{3\theta}{2}\right] \quad (4)$$

$$\sigma_{XY} = \frac{K_1}{\sqrt{2\pi r}}\cos\frac{\theta}{2}\sin\frac{\theta}{2}\sin\frac{3\theta}{2} \quad (5)$$

To address this limitation, stress intensity factors (SIFs) are employed to provide reliable predictions of fracture behavior. In this context, (r) represents the distance from the crack tip to the nearest calculation point, as illustrated in Fig. 3. The stress components, coordinate system, and crack orientation are also presented. The crack is assumed to lie within the (xz)-plane, with its front aligned along the z-axis.

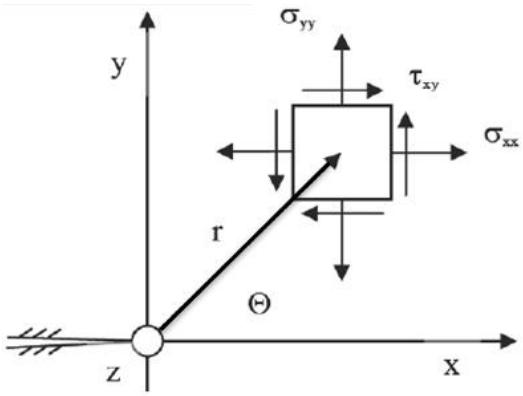

Fig. 3. Distribution of stress components at the tip of a crack

Accurate assessment of a material's fracture behavior depends on determining the stress intensity factor (K). Once (K) is derived, the three primary modes of fracture Mode I (K_1), Mode II (K2), and Mode III (K3) can be evaluated, as shown in Fig. 4. Equations (3), (4), and (5) define the expressions for the stress intensity factor (K1) under various loading conditions. While the stresses at the crack tip theoretically diverge to infinity, the use of SIFs offers a practical means to characterize the fracture response accurately. This framework provides essential insights into the propagation and failure mechanisms of cracked structures under different loading scenarios.

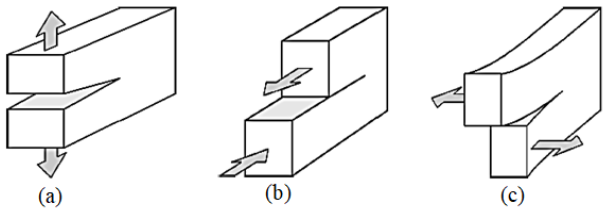

Fig.4. The Three Fundamental Modes of Crack Tip Deformation: (a) Mode I - Opening; (b) Mode II - Sliding; (c) Mode III – Tearing

Fracture toughness measures a material's resistance to brittle failure when a crack is present, indicating the stress needed to propagate flaws like cracks, voids, or weld defects. Linear elastic fracture mechanics (LEFM) is commonly used in the design of critical components, assuming such flaws. Irwin and his colleagues introduced the stress intensity factor (K1), which quantifies fracture toughness by characterizing the stress near the crack tip, affected by residual and applied loads. For mode-I fractures (opening mode), the stress intensity factor K_1 predicts crack propagation and defines the stress field around the crack. For the plate is subsequently determined as [31].

$$K_1 = \sigma\sqrt{\pi a} \quad (6)$$

In functionally graded materials (FGMs), the general form of the stress intensity factor reflects the variation in material properties throughout the component. The expression you provided captures this dependency, ensuring that the stress intensity factor accurately represents the influence of the material gradient The stress intensity factor K_1 quantifies the stress near a crack tip and depends on the applied stress σ, crack length a, and a correction function $f\left(\frac{a}{w}\right)$ as show in Fig. 2 and equation 4 [32].

$$K_1 = f\left(\frac{a}{w}\right)\sigma\sqrt{\pi a} \quad (7)$$

The correction function $f\left(\frac{a}{w}\right)$ Center crack, length 2a in plate of width W as shown in the equation (5) [31]:

$$f\left(\frac{a}{w}\right) = \sigma\sqrt{W\tan\frac{\pi a}{W}} \quad (8)$$

3. NUMERICAL MODEL OF THE CRACKED PLATE

3.1. Geometry of the model

The numerical model consists of a functionally graded material (FGM) plate made of ceramic and metal, as shown in Fig. 5. Width W = 125mm, Height h = 250mm, Thickness e = 2mm. FGM structure changes material properties from ceramic top to metal bottom to resist crack and increase durability. This slow change reduces stress buildup and the plate is better at stopping crack from spreading and lasting longer [33]. The plate is subjected to stress test at 3 levels: 50 MPa, 100 MPa and 150 MPa. FGM plate mechanical properties (Young's modulus and Poisson's ratio) in Tab. 1 [30].

Tab. 1. Material properties of metal and ceramic

Material	Young's modulus (GPa)	Poisson's ratio	Mass density (kg/m^3)
Aluminum (Al)	70	0.3	2702
Zirconia (ZrO_2)	151	0.3	3000

These are the inputs for modeling the material behavior under different loads and crack propagation. The calculations use USDFLD subroutine in Abaqus to update material properties in real time based on field variables during the analysis [34]. Also mixed approach is used to account for the gradual change of material properties.

The aim of these simulations is to study stress, crack initiation and crack propagation under different applied stresses, to get more insight into the structural performance and crack resistance of FGM plates. This study also provides more understanding of FGMs in real life and the potential of advanced FEM, material modeling and multi-objective optimization using NSGA−II for designing crack

DOI 10.2478/ama-2025-0087

resistant structures.

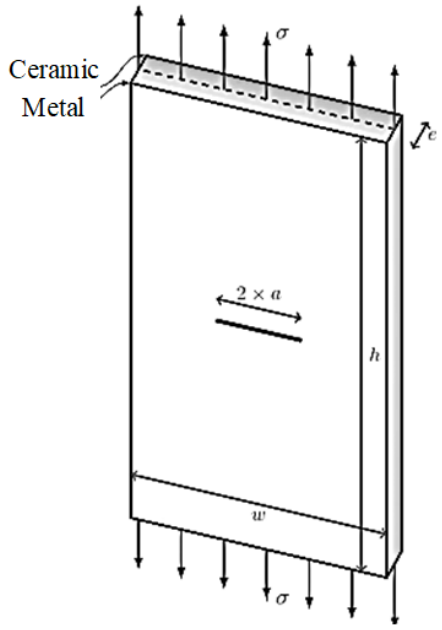

Fig. 5. The material gradient plate (FGM)

3.2. Validation of FEM

Figure 6 presents a comparison between numerical and analytical results for the stress intensity factor (K1) under different applied stresses (50 MPa, 100 MPa, and 150 MPa) as a function of crack length (a). Both methods exhibit similar trends, confirming a consistent relationship between the crack length and the stress intensity factor. However, small discrepancies appear, particularly at larger crack lengths (beyond 20 mm), where the numerical results tend to be slightly lower than the analytical ones. This deviation could be attributed to simplifying assumptions in the analytical model, while the numerical solution might better capture stress concentration effects at the crack tip through mesh refinement.

As expected from Linear Elastic Fracture Mechanics (LEFM), increasing the applied stress results in higher (K1) values. The numerical and analytical results show close agreement at lower crack lengths, but at larger lengths, the differences become more noticeable. For an applied stress of 50 MPa, both solutions start at lower (K1) values, with the numerical approach appearing slightly more conservative. Starting from the stress level of 100 MPa, the numerical and analytical curves begin to diverge at about 15 mm in crack length. At 150 MPa, the divergences in result are most heavy, which may demonstrate an ability for a numerical method to capture complexities such as crack-tip plasticity and geometric effects. This agrees with previous fracture mechanics studies, such as those by [35,36], which have established that for complex geometries or boundary conditions, numerical models often give more accurate results. Furthermore, (Kirthan et al, 2014) [37] noted that the rate of crack growth increases with increased levels of stress, as shown by the increasing values of (K1) in this figure. Increase in the applied stress as well as the length of the crack increases the stress amplification at the crack tip, hence the exponential growth of K1, as observed in the literature. Overall, the numerical model seems to be more conservative for shorter crack lengths and may hence be advantageous in safety-critical applications, whereas the analytical method has a tendency to slightly overestimate the value of K1 for longer cracks. This means that the numerical methods are closer to reality in tackling real-life complexities, particularly regarding the crack-tip stress concentration of components under intense stress.

The developed three-dimensional numerical model investigates a cracked Al2024 T3 plate repaired with a carbon-epoxy composite patch. Finite element modeling requires an appropriate mesh, particularly around the crack tip where stress and strain gradients are significant. The global mesh employs C3D8 elements (8-node linear brick elements). To accurately represent the displacement field near the crack tip, singular elements exhibiting a $1/\sqrt{r}$ singularity are used by shifting the intermediate nodes closer to the crack tip, in accordance with Abaqus software recommendations. Consequently, the mesh around the crack tip is highly refined. For our model, the Functionally Graded Material (FGM) plate adopts the same material parameters as the aluminum plate. The total number of elements depends on the patch shape; for instance, in the case of a rectangular patch, the number and size of elements for each structural component (aluminum plate, crack front, FM-73 adhesive, composite patch) are detailed. Element sizes range from 2 mm in regions far from the crack to approximately 0.078 mm near the crack tip, and remain consistent across all simulations to avoid mesh-related influence on the results. The adhesive is modeled as a third material to account for its actual mechanical properties. The interaction between the adhesive and the cracked plate region, as well as between the composite patch and the adhesive, is assumed to be perfectly bonded (i.e. the two bodies are considered welded during simulations). Symmetry allows modeling only one quarter of the structure, significantly reducing computation time. The boundary conditions applied to the analyzed plate (Fig. 6).

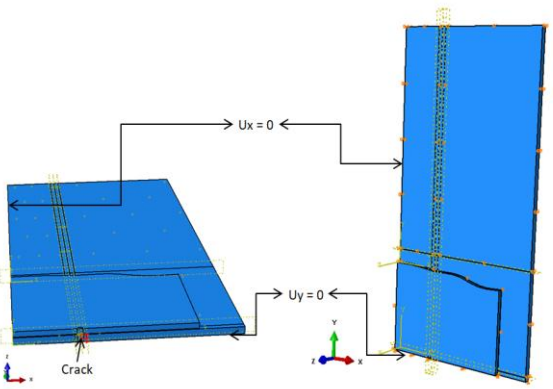

Fig. 6. Boundary conditions imposed on the structure

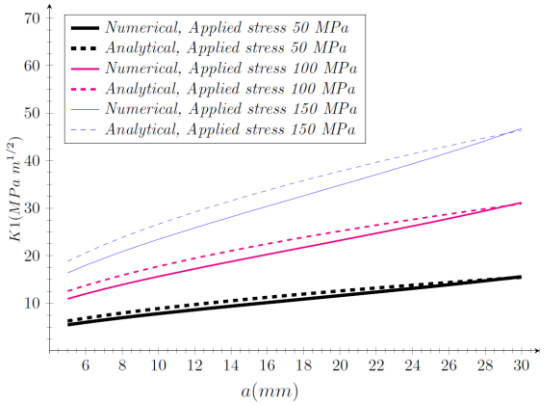

Fig. 7. Comparison of Numerical and Analytical Stress Intensity Factors (K1) at Different Applied Stress Levels

3.3. FEM with carbon fiber-reinforced polymers (CFRP) patch

This study focuses on the analysis of a reinforced plate structure, utilizing the principle of symmetry to reduce computational time by examining only half of the model. The plate is characterized by dimensions of $W = 125/2\ mm$ in width, $H = 250/2\ mm$ in height, and $e = 125/2\ mm$ in thickness. An initial crack, with a total length of $2a = 36mm$, is located at the center along the longer dimension of the plate. The adhesive layer applied to the structure has a thickness of $e_a = 0.2\,mm$, while the patch thickness is $e_r = 1.5\,mm$. In-plane coordinates along the x-axis are defined as $x_i = [0,10,20,30,40,50]\text{mm}$, with corresponding y_i values randomly generated between 10 and 40mm, introducing spatial variability to the analysis. The mechanical properties of both the adhesive and the carbon fiber composite patch are detailed in Tab. 2. To simulate realistic loading conditions, a uniform pressure of 150 MPa is applied across the plate.

Functionally Graded Materials are advanced composites that exhibit a gradual transition in material properties, enhancing mechanical performance by integrating the strengths of different materials. In this study, the plate consists of ceramic and metal layers. The ceramic layer on the top provides exceptional wear and thermal resistance, while the metallic base offers ductility and damage tolerance. Fig. 8 illustrates the use of Carbon Fiber-Reinforced Polymer (CFRP) patches to repair or reinforce the plate in areas prone to cracking. CFRP is commonly employed in structural repairs due to its high strength-to-weight ratio, corrosion resistance, and ease of application. The non-uniform patch profile emphasizes the importance of optimizing patch geometry to reduce stress concentrations, thereby improving the fatigue life of the repaired component. A set of measurement points (x0) to (x5) is distributed along the x-axis, spaced at 10 mm and 50 mm intervals, highlighting regions of interest for stress analysis.

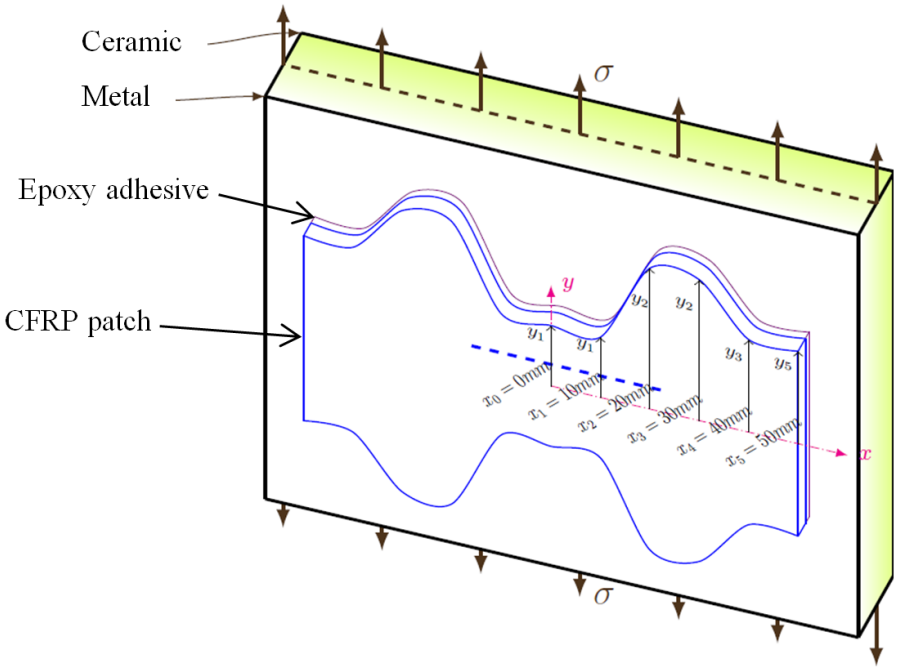

Fig. 8. FGM Plate Reinforced with Carbon Fiber-Reinforced Polymer (CFRP) Patches under Tensile Loading with Ceramic-Metal Gradient Layers and Patch Optimization Paths

Tab. 2. Mechanical properties of composite patch and adhesive

	Composite patch	Adhesive
$E_1(\text{GPa})$	135	2.1547
$E_2(\text{GPa})$	9	
$E_3(\text{GPa})$	9	
$G_{12}(\text{GPa})$	5	
$G_{13}(\text{GPa})$	5	
$G_{23}(\text{GPa})$	8	
ν_{12}	0.3	0.34
ν_{13}	0.3	
V_{23}	0.02	

The contour lines indicate varying crack growth paths or stress distributions under loading. Along the thickness of the plate, several points are marked (y_1 , y_2 , ..., y_6) where the stress intensity factors (SIFs) could be evaluated, which is essential for understanding crack propagation behavior in layered materials. The applied tensile stress σ, indicated by vertical arrows on both surfaces, creates a loading scenario that mimics real-life conditions where FGMs might experience mechanical stress. The interaction between the layered FGM structure and the CFRP patch aims to optimize stress transfer while minimizing crack growth and preventing structural failure.

DOI 10.2478/ama-2025-0087

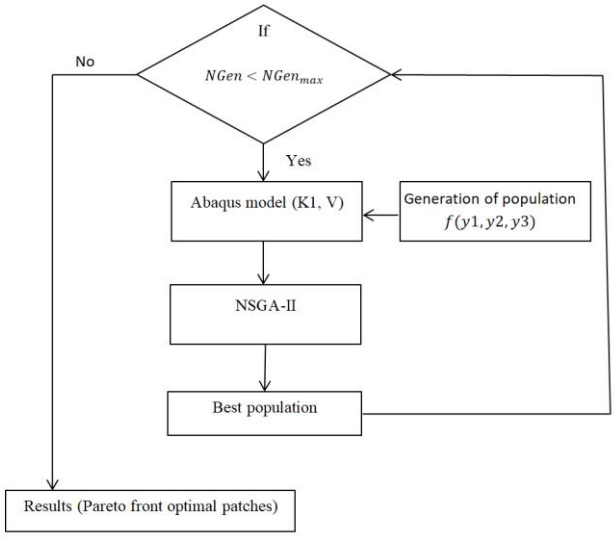

Fig. 9. Optimization Flowchart Using NSGA-II and Pareto Front Method to Identify Optimal Patch Geometries through Abaqus Simulations

Fig. 9 Flowchart of the optimization process using NSGA−II to obtain the optimal patch geometries from Pareto front. This is necessary when dealing with multi-objective problems such as minimization of K_1 and maximization of V for better performance of the patch. It does this by first generating a population of possible solutions with parameters; these parameters will most likely be geometric dimensions or material properties of the patch. The population is allowed to evolve through generations, with Abaqus modeling and evaluating each solution for K_1 and V in orde to measure its performance. In each iteration, NSGA−II evaluates the population, ranking solutions based on non-dominance. The best population from each generation is selected and refined through this evolutionary approach. The loop continues as long as the number of generations (NGen) is less than the maximum allowed generations $(NGen_{max})$. When the maximum number of generations is reached or the algorithm converges, the process yields the Pareto front a set of non-dominated, optimal solutions. This front represents the best trade-offs between conflicting objectives, such as minimizing stress while maintaining patch volume, providing insight into the most effective patch geometries.

The NSGA−II (Non-dominated Sorting Genetic Algorithm II) method is a multi-objective optimization algorithm widely used to solve complex problems where multiple, often conflicting objectives need to be optimized simultaneously. The algorithm starts by generating an initial population P_t, then creates a population Q_t by applying genetic operators such as selection, crossover, and mutation. These two populations are merged to form R_t, a combined population. Then, R_t is sorted into several fronts F1, F2,.., using a Pareto dominance-based sorting: front F1 contains the non-dominated solutions, followed by the successive fronts F2, F3, etc. Within each front, a measure called crowding distance is used to assess the diversity of solutions. Individuals are prioritized to ensure a good distribution of solutions on the Pareto front. The new population Pt+1 is then formed by selecting individuals from the successive fronts until the maximum population size is reached, giving priority to those who contribute to the diversity if necessary (Fig. 10). These steps are repeated until the stopping criterion is met [38].

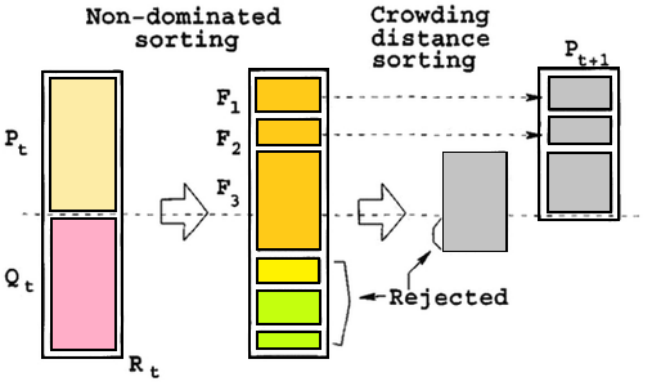

Fig. 10. Flowchart of the NSGA-II Multi-Objective Optimization Process for Patch Geometry and Stress Intensity Factor Minimization

The optimization of the proposed model relies on determining the optimal geometric parameters of a patch, defined by the input vector y1 , y2 , y3 . In this vector, y1 , y2 , and y3 represent the ordinates describing the shape of the patch, while a corresponds to the crack length. The goal of this optimization is to simultaneously minimize two main outputs: the patch volume and the stress intensity factor K_1 , which measures the effect of the crack on local stresses. To achieve this goal, a multi-objective optimization approach is employed, enabling the search for an optimal balance between these two criteria. Minimizing the patch volume aims to reduce the amount of material needed, contributing to the efficiency and lightness of the solution. At the same time, reducing K1 is essential for improving the durability and mechanical strength of the structure by limiting crack propagation.

4. RESULT AND DISCUSSION

4.1. Influence of η_c and η_m

The optimal combination of parameters η_c and η_m, as depicted in Fig.11, occurs when both parameters have moderate to high values, such as η_c = 2 and η_m = 10. This combination allows for a good trade-off between reducing the patch volume and minimizing the stress intensity factor K1 while maintaining sufficient diversity in the solutions. A higher value of ηc seems to accelerate the reduction of volume without significantly compromising K_1 performance, thus widening the Pareto front by offering a range of optimal solutions. Therefore, this combination provides a balanced and effective set of solutions, maximizing repair performance while keeping the patch volume minimal. The Non-dominated Sorting Genetic Algorithm II (NSGA−II) was employed to identify optimal solutions along the Pareto front, balancing tradeoffs between conflicting objectives, such as minimizing degradation while maintaining structural stability [39].

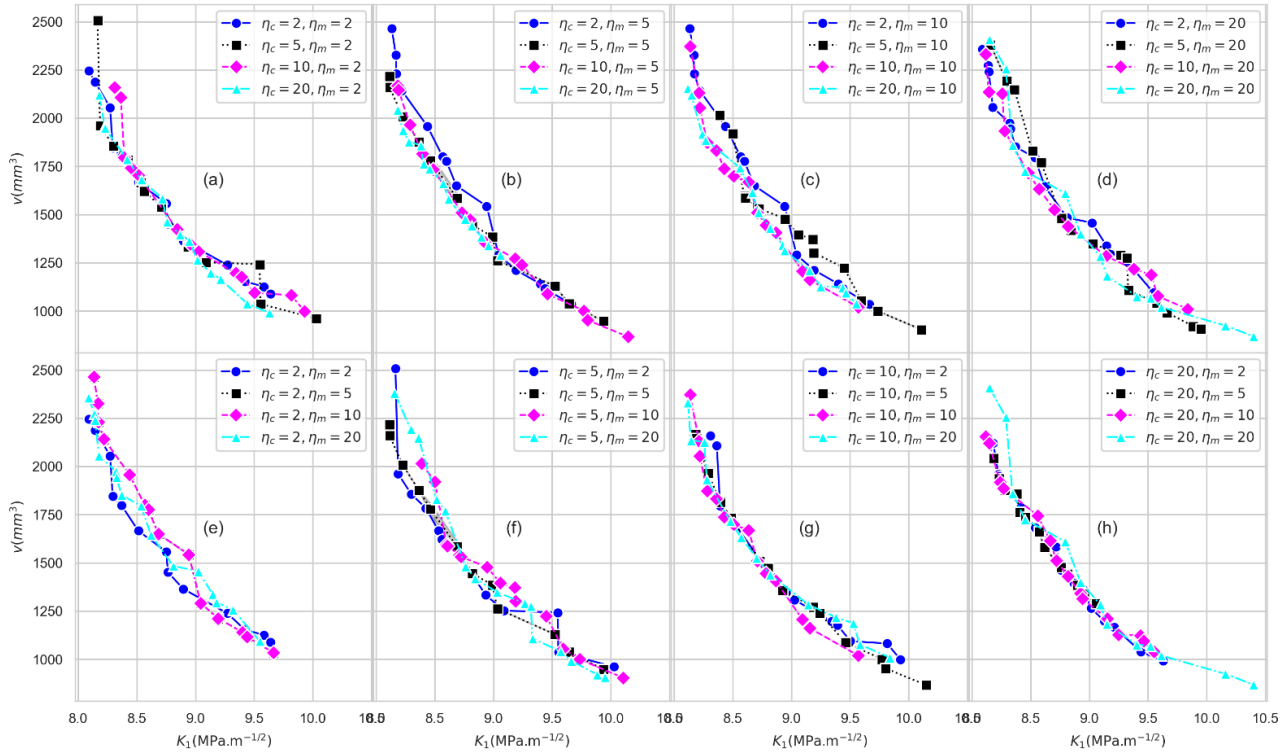

Fig. 11. Influence of Parameters η_c and η_m on Volume Reduction (V) as a Function of (k_1) with NSGA-II Pareto Front Optimization.

4.2. Influence of number of population

The evolution of the Pareto front using NSGA−II optimization for varying population sizes (10, 20, 30, 40, 50, and 60) demonstrates the trade-off between volume V and K1. As illustrated in Fig. 12, each plot captures the spread of solutions over 10 generations, with distinct colors representing the progression across generations.

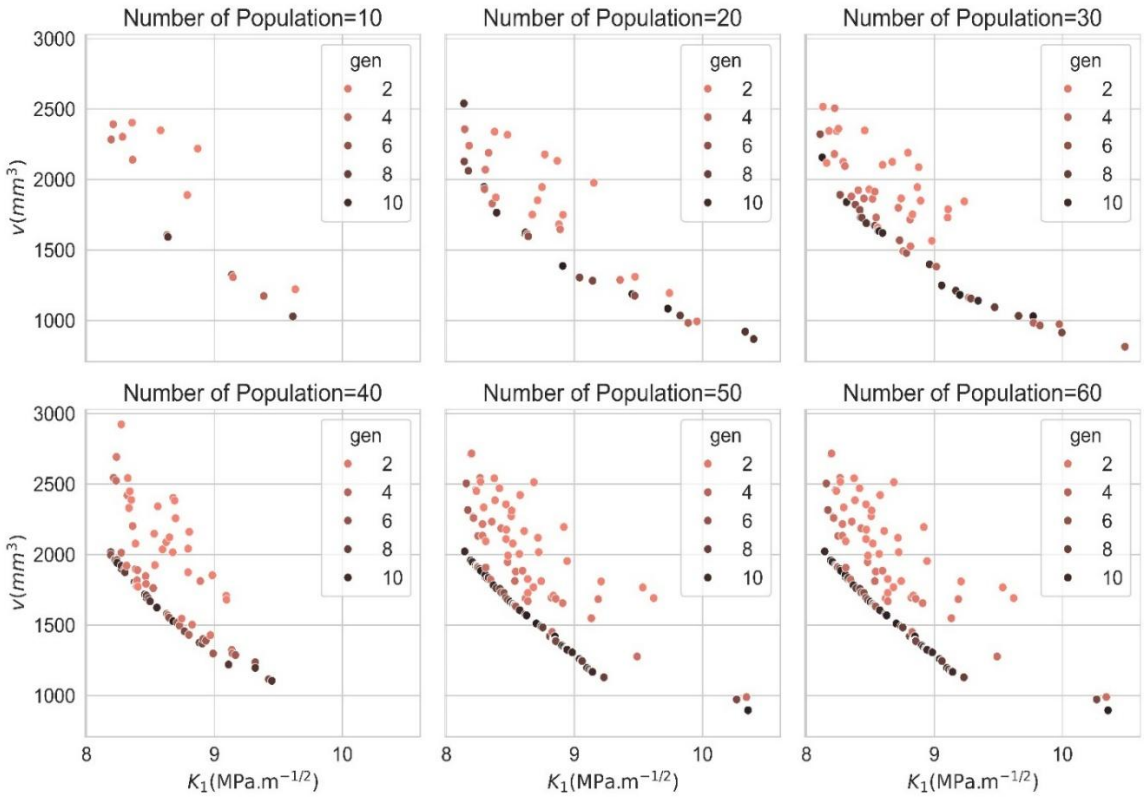

Fig. 12. Evolution of the Pareto Front with NSGA-II Optimization for Different Population Sizes

DOI 10.2478/ama-2025-0087

It is evident that population size significantly affects both the convergence and diversity of the Pareto front. At smaller populations (e.g., 10), the solutions are sparse, limiting the algorithmics ability to explore the solution space effectively. As the population size increases to 20, the Pareto front becomes well-defined and expands across a broader range of (K1) and (V), suggesting a better balance between exploration and exploitation. With further increases in population (30, 40, 50), the solution density along the front improves; however, beyond 20, the marginal gains diminish, leading to redundant solutions and higher computational costs without significant improvements in optimization quality. A population size of 20 provides an optimal balance, ensuring the Pareto front is well-formed while maintaining a wide spread of values for (K1) and (V). This result aligns with prior works, such as Worthington et al. (2023), which demonstrated that increasing population size initially improves convergence but eventually leads to slower optimization with diminishing returns [40]. Similarly, Zhang et al. (2023) emphasized the importance of balancing exploration and exploitation, noting that too small a population hinders convergence, while larger sizes increase computational time unnecessarily [41]. NSGA−II with a population size of 20 offers the most effective trade-off between convergence and solution diversity. Although higher populations (e.g., 40, 50) improve coverage, they also introduce computational inefficiencies with limited improvement in the Pareto front's structure. This study suggests that adaptive population strategies or hybrid algorithms could further optimize performance.

4.3. Influence of number of generations

To determine the optimal number of generations for our model, we initially set the population size to 20 individuals. As illustrated in Fig.13, the algorithm demonstrates noticeable convergence after approximately 20 generations. To ensure robust and reliable results, we extended the number of generations to 30 for the remaining calculations, allowing the model to achieve a stable solution without unnecessary computational overhead.

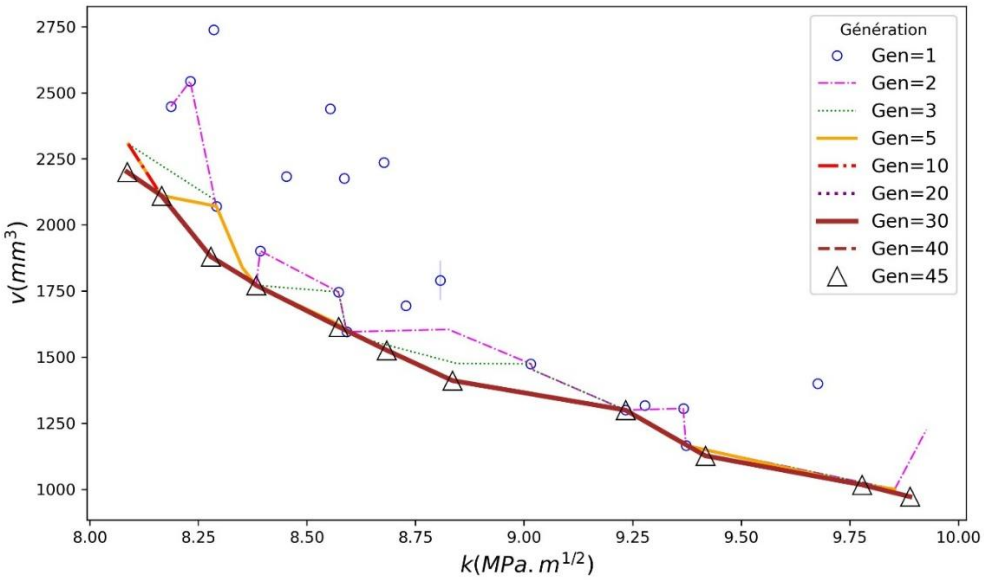

Fig. 13. Convergence of the NSGA-II Algorithm with Respect to the Number of Generations

4.4. Patch dashboard based on volume and stress intensity factor K_1

Figure 14 shows the relationships between patch width (W_p), patch height (h_p), stress intensity factor K1 , and patch volume V in the patch optimization dashboard. Configurations in this figure are Pareto-optimal solutions that other the best trade-offs between material usage and stress reduction. To enable comparisons of different designs more easily, a normalized parameter is defined, Pvk = (v /k1 /100), which enhances flexibility for engineers to choose configurations according to specific goals, such as minimum material use or maximum reduction of stresses. The dashboard also shows the variation in crack length (10mm, 18mm and 26mm) in the optimization process. This presents a more complete approach compared to other studies by combing Abaqus simulations with multi-objective optimization using NSGA−II. In the case of conventional optimization techniques, they are usually performed by using deterministic methods or trial-and-error approaches by using infnite element methods (FEM), which limit the search for the solution space. By contrast, NSGA−II finds a set of non-dominated solutions that show a better set of volume-K1 trade-offs and provide the decision-maker with an enhanced perspective. It considers some critical enhancements over previous literature. For instance, (Yang et al, 2024) [22] proposed the optimization of patch designs through the use of the stop-hole technique; their reliance on manual parameter tuning hindered the efficiency of the simulations themselves. Using the technique of NSGA−II, our method gives a Pareto front of optimal solutions without manual intervenetion. Meanwhile, genetic algorithms were used by (Poirier et al, 2013) [42] in single-objective optimization, either minimizing volume or reducing stress concentration, but our work extends the previous research by tackling both objectives simultaneously and presenting those solutions interactively. The proposed approach of coupling FEM simulations with NSGA−II not only accelerates the optimization process but also effectively provides the optimal solutions. The major advantage of this approach is the dynamic selection of Pareto-optimal solutions, thus enabling the engineers to make choices in designing patches that satisfy specific constraints. The introduction of the parameter Pvk opens up new avenues for the comparison of patches in view

of sustainable use of materials with no compromise on crack resistance. The search for Pareto-optimal solutions means less computational effort because fewer unnecessary simulations are required; thus, time and resources are saved. The present study represents the first attempt to integrate FEM simulations with multi-objective optimization using NSGA−II. It provides a solution for crack repair that is workable, efficient, and sustainable through combining flexible solution selection, interactive visualization, and the innovatory parameter. This work makes a valuable contribution to fatigue crack repair in metals and especially to the discipline of repair optimisation, enhancing the effectiveness and efficiency of optimization in patch design compared to methodologies that have thus far been followed.

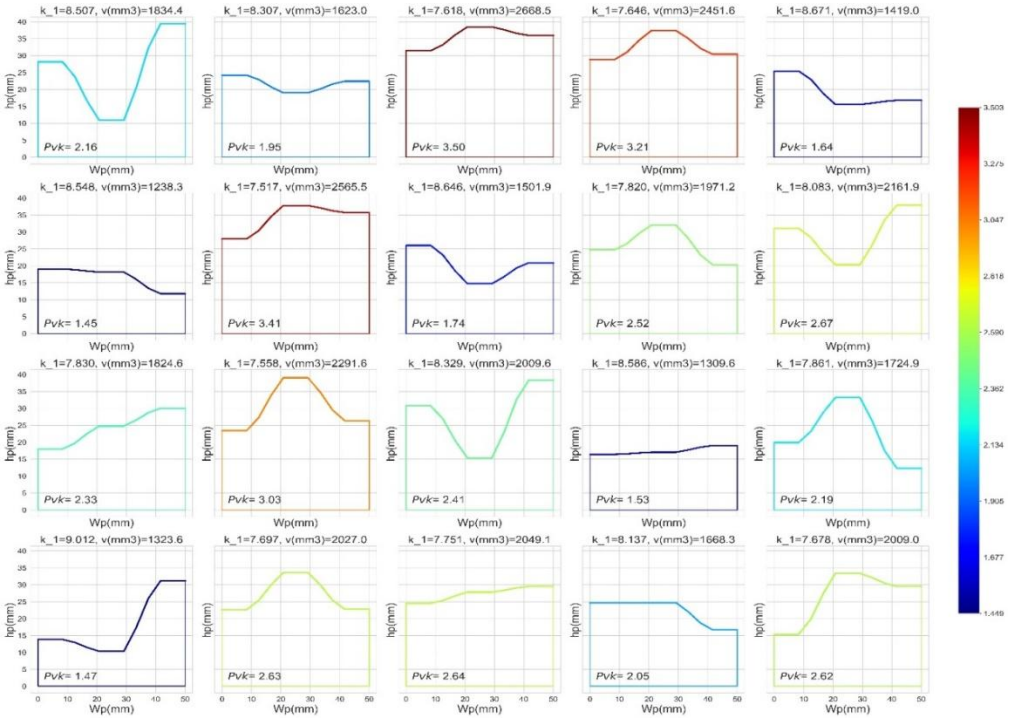

(a)

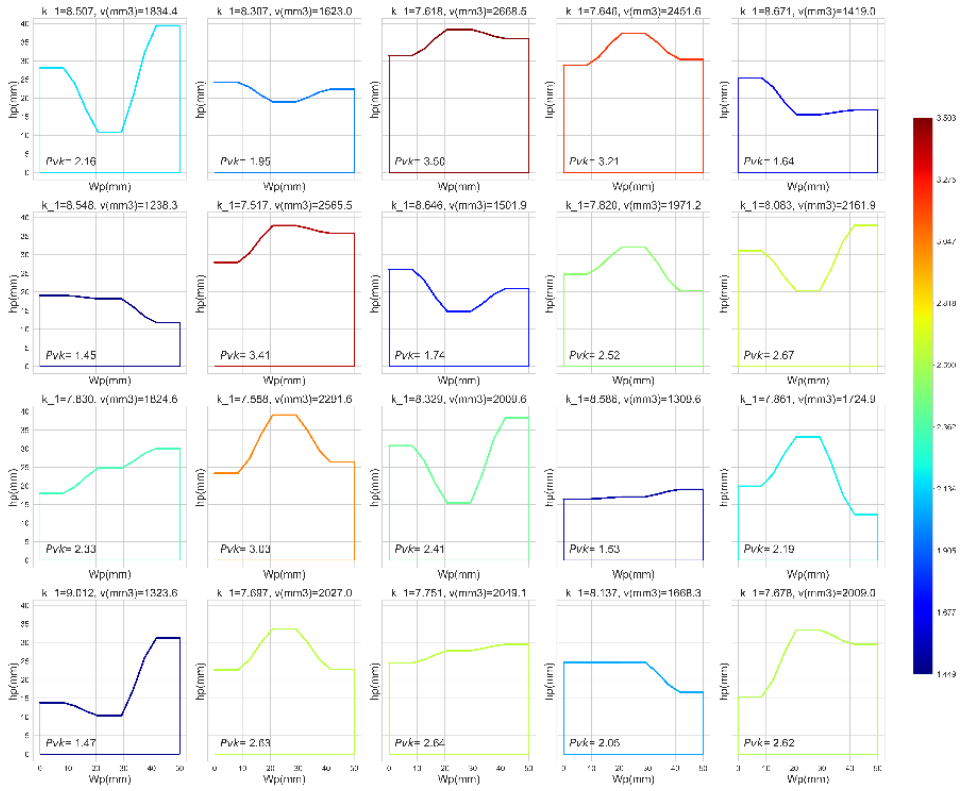

(b)

DOI 10.2478/ama-2025-0087

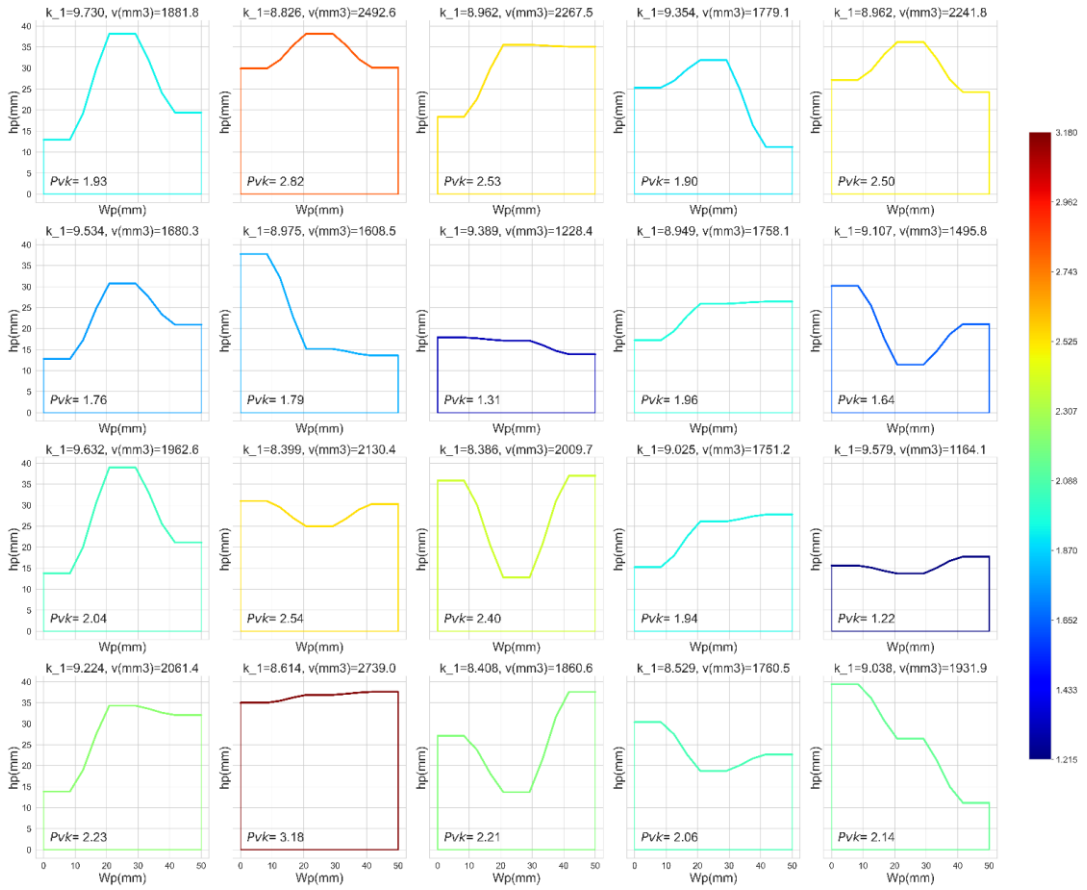

(c)

Fig. 14. Patch Dashboard for Multi-Objective Optimization of Crack Repair: Trade-offs Between Volume and Stress Intensity Factor (K_1); a) 2a=10 mm, b) 2a=18mm, c) 2a=26mm

5. CONCLUSION

In this work, the patch shape of a functionally graded material plate is optimized using the Non-dominated Sorting Genetic Algorithm II. The major goal of the study is to minimize mode I stress intensity factor, K1 , that plays a significant role in the determination of crack propagation. Different trade-offs were investigated by utilizing the Pareto front, and the optimal crack shapes for repair were identified. Optimization resulted in a number of important results:

- The optimized patch shapes reduced the mode I stress intensity factor K_1, which means a significant improvement in the plate resistance to crack propagation.
- Several configurations of effective patches were found, which show that certain geometries can effectively distribute the stress and reduce crack growth.
- The Pareto front analysis highlighted the trade-offs among different design parameters, facilitating informed decision-making with respect to optimal shapes.
- The Pareto front highlighted the trade-offs for various design parameters and hence allowed making an informed decision on optimum shapes.
- These shapes obtained were chosen as the optimum since they minimized not only K_1 but generally improved the performance of the FGM plate in different loadings.
- Moreover, it allows the possibilities of taking up more variables that can affect

REFERENCES

1. Van Doan D, Van Minh P, Van Ke T, Nhung NTC, Van Thom D. An overview of functionally graded materials: from civil applications to defense and aerospace industries. J Vib Eng&Technol. 2025;13(1):68.
2. Hussain SA, Charoo MS, Haq MIU. 3D printing of functionally graded materials: Overcoming challenges and expanding applications. In: Multi-material Additive Manufacturing. Elsevier. 2025; 67–97.
3. Alkunte S, Fidan I, Naikwadi V, Gudavasov S, Ali MA, Mahmudov M, et al. Advancements and challenges in additively manufactured functionally graded materials: A comprehensive review. J Manuf Mater Process. 2024;8(1):23.
4. Kumar P, Sharma SK, Singh RKR. Recent trends and future outlooks in manufacturing methods and applications of FGM: a comprehensive review. Mater Manuf Process. 2023;38(9):1033–67.
5. Li Y, Feng Z, Hao L, Huang L, Xin C, Wang Y, et al. A review on functionally graded materials and structures via additive manufacturing: from multi-scale design to versatile functional properties. Adv Mater Technol. 2020;5(6):1900981.
6. Saleh B, Jiang J, Fathi R, Al-Hababi T, Xu Q, Wang L, et al. 30 Years of functionally graded materials: An overview of manufacturing methods, Applications and Future Challenges. Compos Part B Eng. 2020;201:108376.
7. Sun L, Sneller A, Kwon P. Fabrication of alumina/zirconia functionally graded material: From optimization of processing parameters to phenomenological constitutive models. Mater Sci Eng A. 2008;488 (1–2):31–8.

8. Hvizdoš P, Jonsson D, Anglada M, Anné G, Van Der Biest O. Mechanical properties and thermal shock behaviour of an alumina/zirconia functionally graded material prepared by electrophoretic deposition. J Eur Ceram Soc. 2007;27(2–3):1365–71.
9. Huang CY, Chen YL. Effect of varied alumina/zirconia content on ballistic performance of a functionally graded material. Int J Refract Met Hard Mater. 2017;67:129–40.
10. Beranič Klopčič S, Novak S, Kosmač T, Richter HG, Hecht-Mijic S. The preparation and properties of functionally graded alumina/ zirconia-toughened alumina (zta) ceramics for biomedical applications. Key Eng Mater. 2005;290:348–52.
11. Bhattacharya S, Sharma K. Fatigue crack growth simulations of FGM plate under cyclic thermal load by XFEM. Procedia Eng. 2014;86: 727–31.
12. Sun L, Grasselli G, Liu Q, Tang X. Thermal cracking simulation of functionally graded materials using the combined finite--discrete element method. Comput Part Mech. 2020;7:903–17.
13. Lesiuk G, Katkowski M, Duda M, Królicka A, Correia J, De Jesus AMP, et al. Improvement of the fatigue crack growth resistance in long term operated steel strengthened with CFRP patches. Procedia Struct Integr. 2017;5:912–9.
14. Tavakkolizadeh M, Saadatmanesh H. Fatigue strength of steel girders strengthened with carbon fiber reinforced polymer patch. J Struct Eng. 2003;129(2):186–96.
15. Hu J, Kang R, Fang J, Chen S, Xuan S, Zhou J, et al. An experimental and parametrical study on repair of cracked titanium airframe structures with single-side bonded carbon fiber-reinforced polymer prepreg patches. Compos Struct. 2024;338:118102.
16. Karuppannan D, Rawat RS, Ramachandra H V, Saji D, Varughese B. Composites for reinforcement of damaged metallic aircraft wings. J Aerosp Sci Technol. 2013;8–13.
17. Brandtner-Hafner M. Evaluating the bonding effectiveness of CFRP patches in strengthening concrete structures. Constr Build Mater. 2024;436:136966.
18. Reis JML, Costa AR, da Costa Mattos HS. Repair of damage in pipes using bonded GFRP patches. Compos Struct. 2022;296:115875.
19. El-Emam HM, Salim HA, Sallam HEDM. Composite patch configuration and prestraining effect on crack tip deformation and plastic zone for inclined cracks. J Compos Constr. 2016; 20(4):4016002.
20. Ghafoori E, Motavalli M. A retrofit theory to prevent fatigue crack initiation in aging riveted bridges using carbon fiber-reinforced polymer materials. Polymers (Basel). 2016;8(8):308.
21. Boulenouar A, Bouchelarm MA, Chafi M. Numerical investigation of cracked metal/ceramic FGM plates repaired with bonded composite patch. Int J Interact Des Manuf. 2024;18(2):649–58.
22. Yang X, Wu Z, Zheng J, Lei H, Liu L, Chen W. Multi objective optimization of composite laminate repaired by patches in considering static strength and fatigue life. Mech Adv Mater Struct. 2024;1–21.
23. Peng X, Guo Y, Li J, Wu H, Jiang S. Multiple objective optimization design of hybrid composite structures considering multiple-scale uncertainties. Compos Struct. 2022;292:115658.
24. He Y, Lu D, Li Z, Lu D. Multi-objective optimization of the low-pressure casting of large-size aluminum alloy wheels through a systematic optimization idea. Materials (Basel). 2023;16(18):6223.
25. Wang G, Deng J, Lei J, Tang W, Zhou W, Lei Z. Multi-Objective Optimization of Laser Cleaning Quality of Q390 Steel Rust Layer Based on Response Surface Methodology and NSGA-II Algorithm. Materials (Basel). 2024;17(13):3109.
26. Limmun W, Chomtee B, Borkowski JJ. Robust D-Optimal Mixture Designs Under Manufacturing Tolerances via Multi-Objective NSGA-II. Mathematics. 2025;13(18):2950.
27. Wang Q, Wang L, Huang W, Wang Z, Liu S, Savić DA. Parameterization of NSGA-II for the optimal design of water distribution systems. Water. 2019;11(5):971.
28. Liu Y, Meng J, Li T. Structural Optimization of a Giant Magnetostrictive Actuator Based on BP-NSGA-II Algorithm. In: Actuators. 2024; 293.
29. Reddy J. Analysis of functionally graded plates. Int J Numer Methods Eng. 2000;47(1-3):663–84.
30. Nguyen TK. A higher-order hyperbolic shear deformation plate model for analysis of functionally graded materials. Int J Mech Mater Des. 2015;11:203–19.
31. Alam MM, Barsoum Z, Jonsén P, Häggblad HÅ, Kaplan A. Fatigue behaviour study of laser hybrid welded eccentric fillet joints: Part II: State-of-the-art of fracture mechanics and fatigue analysis of welded joints. In: Nordic Conference on Laser Processing of Materials: 24/08/2009-26/08/2009. 2009.
32. Kumar B, Sharma K, Kumar D. Evaluation of stress intensity factor in functionally graded material (FGM) plate under mechanical loading. Indian Soc Theor Appl Mech (ISTAM), Jaipur; 2015.
33. Baghdadi M, Serier B, Salem M, Zaoui B, Kaddouri K. Modeling of a cracked and repaired Al 2024T3 aircraft plate: effect of the composite patch shape on the repair performance: Effect of the composite patch shape on the repair performance. Frat ed Integrità Strutt. 2019;13(50):68–85.
34. Chama M, Moulai-Khatir D, Hamza B, Slamene A, Mokhtari M. Novel FGM-USDFLD approach in Graded Cohesive Zone Modeling (GCZM): Predicting debonding and crack propagation in composite-patched notched plates. Mech Adv Mater Struct. 2024;1–16.
35. Peng X, Atroshchenko E, Kerfriden P, Bordas S. Isogeometric boundary element methods for three dimensional static fracture and fatigue crack growth. Comput Methods Appl Mech Eng. 2017;316:151–85.
36. Roychowdhury S, Dodds Jr RH. A numerical investigation of 3-D small-scale yielding fatigue crack growth. Eng Fract Mech. 2003;70(17):2363–83.
37. Kirthan LJ, Hegde R, Suresh BS, Kumar RG. Computational analysis of fatigue crack growth based on stress intensity factor approach in axial flow compressor blades. Procedia Mater Sci. 2014;5:387–97.
38. Deb K. Mutliobjective Optimization using Evolutionary Algorithms. Journal of Physics A: Mathematical and Theoretical. 2011;44: 1689–1699.
39. Deb K, Pratap A, Agarwal S, Meyarivan T. A fast and elitist multiobjective genetic algorithm: NSGA-II. IEEE Trans Evol Comput. 2002;6(2):182–97.
40. Worthington M, Chew HB. Crack path predictions in heterogeneous media by machine learning. J Mech Phys Solids. 2023;172:105188.
41. Zhang S, Li R, Lu D, Xu L, Xu W. Multi-objective optimization design of assembled wheel lightweight based on implicit parametric method and modified NSGA-II. IEEE Access. 2023;11:71387–406.
42. Poirier JD, Vel SS, Caccese V. Multi-objective optimization of laser-welded steel sandwich panels for static loads using a genetic algorithm. Eng Struct. 2013;49:508–24.

Soufiane Abbas: https://orcid.org/0009-0009-7485-0407

Mohamed Ikhlef Chaouch: https://orcid.org/0000-0002-9486-1893

Hinde Laghfiri: https://orcid.org/0000-0002-4296-9165

Mohamed Benguediab: https://orcid.org/0000-0002-6595-5786